MODELLING AND EFFICIENCY OPTIMISATION OF SINGLE-JUNCTION INGAP SOLAR CELLS

ALA'EDDIN A. SAIF

Department of Physical Sciences, College of Science, University of Jeddah, Jeddah, Saudi Arabia E-mail: aasaif@uj.edu.sa

Abstract

This study aims to optimise the photovoltaic properties of the single-junction In_{0.49}Ga_{0.51}P solar cell by systematically adjusting the doping levels and the thickness of various cell layers using Silvaco TCAD simulation software. To improve the cell performance, materials with large energy bandgaps, particularly AlGaAs and AlGaInP, are used as the window and back surface field (BSF) layers, respectively. A wide range of doping concentrations and thickness variations for each solar cell layer have been investigated to determine the best combinations for maximising the cell's efficiency and overall photovoltaic performance. The results show that the $J_{\text{sc}},\,V_{\text{oc}},\,P_{\text{max}},\,FF,$ and η enhanced from 17.44 mA/cm², 1.27 V, 18.4 mW/cm², 82.95%, and 18.43% for the initial proposed cell to 25.8 mA/cm², 1.38 V, 32.05 mW/cm², 90.24%, and 32.09% for the optimised cell, respectively. This confirms the impact of adjusting the doping concentration and thickness of the cell's layers on the cell performance. The solar cell's outstanding efficiency in this study is ascribed to the AlGaInP BSF layer's involvement in the confinement of the photogeneration carriers, augmenting the overall photocurrent. EQE and IQE significantly improve after optimising the emitter and base areas compared to the other layers within the corresponding bandgap wavelengths.

Keywords: InGaP solar cell, Quantum efficiency, Recombination, Silvaco TCAD.

1. Introduction

Photovoltaic is the most extensively utilised and developed renewable energy technology. It has been identified as one of the most promising options for reducing the demand for fossil fuels in various applications [1]. Due to the semiconductor structure of III-V compounds, they absorb a sizeable portion of the solar spectrum; thus, III-V solar cells will continue to receive extensive efforts to increase their efficiency [2]. In_{0.49}Ga_{0.51}P solar cells have a direct and relatively large energy bandgap of 1.9 eV; therefore, they have been employed as an upper cell for heterojunction solar cells such as InGaP/GaAs [3, 4], InGaP/GaAs/Ge triple-junction solar cells [5], and InGaP /Si multi-junction solar cells [1, 6]. The upper InGaP solar cell captures the high-energy photons, resulting in the absorption of the lower-energy photons by the cell underneath. Furthermore, InGaP has a high absorption coefficient and is non-toxic, inexpensive, and thermally stable, all of which are advantageous when fabricating an environmentally friendly solar cell with high conversion efficiency [7].

A comprehensive review of the existing literature reveals that a limited amount of research has been conducted on the study of single junction InGaP solar cells. Takamoto et al. [8] introduced an experimental work for an InGaP homojunction cell on a GaAs substrate, and they achieved an optimum conversion efficiency of 17%. Chang et al. [9] fabricated a single-junction InGaP solar cell by a microhole array texturing technique and achieved an optimum conversion efficiency of 15.91%. Dai et al. [10] reported a GaInP single-junction solar cell stacked on GaAs substrate by molecular beam epitaxy (MBE) at a high temperature, giving a 16.6% efficiency under AM1.5G illumination. Benlekhdim et al. [11] suggested a model that optimises a single-junction In_{0.49}Ga_{0.51}P solar cell using an AlGaAs window layer and InGaP BSF layer by Silvaco ATLAS to achieve an efficiency of 18.55%. Another model for a single junction In_{0.49}Ga_{0.51}P solar cell is introduced by Verma et al. [12] using the Silvaco ATLAS simulator. The optimum efficiency of 21.59% is obtained when double BSF layers are used. Soley and Dwivedi [13] reported an efficiency of 13.42% for homojunction InGaP solar cells using the Silvaco ATLAS simulator. Recently, in 2024, Charane et al. reported a simulation work via Silvaco TCAD for a single-junction solar cell using Ga_{0.04}In_{0.96}P with an energy bandgap of 1.39 eV and achieving an efficiency of 23.73% [14].

Due to the wide band bandgap of the InGaP, it has received less attention from researchers being used as a single junction solar cell compared to other III-V materials solar cells. Besides the considerable expenses and time-intensive associated with conducting experimental research for the synthesis and optimisation of the InGaP solar cell, it is required to repeat the process until the desired findings are obtained. The current work proposes a configuration of a single-junction In_{0.49}Ga_{0.51}P solar cell using AlGaAs and AlGaInP as the window and back surface field (BSF) layers, respectively. The study is conducted using the SILVACO TCAD simulator, a sophisticated and widely used tool in semiconductor device modelling, to optimise the performance of solar cells. The cell's efficiency has been optimised by varying its regions' doping level and thickness. The solar cell's performance in terms of its electrical parameters, photogeneration and recombination rates, and internal and external efficiency is deeply investigated.

2. Methods

Silvaco-TCAD is widely regarded as a highly reliable semiconductor simulator. Researchers have widely employed solar cell modelling due to its ability to manipulate numerous factors and reduce processing time more cheaply than the production method [11, 12, 15, 16]. The operational mechanism relies on the resolution of mathematical equations, specifically Poisson's formula, continuity equation, and transport equations about carriers.

Poisson's equation relates the generated electric field with charge density and, in one dimension, is given in Eq. (1):

$$\frac{\partial E}{\partial x} = \frac{\rho}{\varepsilon} \tag{1}$$

Since the electric field, E can be expressed in terms of electrostatic potential $(E = -\frac{\partial \Psi}{\partial x})$, Poisson's equation can be written as [17].

$$\frac{\partial^2 \Psi}{\partial x^2} + \frac{q}{\varepsilon} [p(x) - n(x) + N_D + N_A + \rho_p - \rho_n] = 0$$
 (2)

where ε is the permittivity, q is the electronic charge, n is the electron density, N_A is the ionised acceptors' concentration, N_D is the ionised donors' concentration, p is the free hole density, and ρ_n and ρ_n are the distribution of hole and electron.

The hole continuity equation is given by:

$$\frac{1}{q}\frac{\partial J_p}{\partial x} = G_{op} - R(x) \tag{3}$$

The electron continuity equation is given by.

$$\frac{1}{q}\frac{\partial J_n}{\partial x} = -G_{op} + R(x) \tag{4}$$

where G_{op} is the generation rate, and R is the recombination rate.

In semiconductor materials, the drift-diffusion current density of holes and electrons is given by the following equations [17, 18]

$$J_{p} = \frac{\mu_{p} p}{q} \frac{\partial E_{Fp}}{\partial x}$$

$$J_{n} = \frac{\mu_{n} n}{q} \frac{\partial E_{Fn}}{\partial x}$$

$$\tag{5}$$

$$J_n = \frac{\mu_n n}{\sigma} \frac{\partial E_{Fn}}{\partial r} \tag{6}$$

where μ_p is the hole mobility, μ_n is the electron mobility, E_{Fp} is the Fermi level of holes, and E_{Fn} is the Fermi level of electrons.

Figure 1 illustrates the cross-sectional configuration of the initial solar cell in the present study. Each layer is defined by the doping concentration, thickness, and physical parameters, including bandgap energy, relative permittivity, electron affinity, effective density of states, carrier mobilities, and carrier lifetimes. The semiconductor characteristics of the materials are listed in Table 1. The doping concentration and thickness values of the initial cell regions are indicated in Fig. 1. The physical models of AUGER, optr, FERMI, conmob, and bgn have been considered. The cell electrical parameters are evaluated utilising a sequence of extracting expression for the short circuit current density, open circuit voltage, fill factor, and conversion efficiency.

The current density of the solar cells is usually defined using the following expression:

Journal of Engineering Science and Technology December 2024, Vol. 19(6)

$$J = J_{sc} - J_o \left(e^{\frac{qV}{K_B T}} - 1 \right) \tag{7}$$

By setting J = 0, the open circuit voltage of the cell can be given as:

$$V_{oc} = \frac{qV}{K_B T} \ln \left(\frac{J_{sc}}{J_o} + 1 \right) \tag{8}$$

where J_{sc} is the short circuit current density, J_o is the saturation current density, and V is the voltage between the terminals.

The fill factor (FF) is commonly used to denote the squareness of the IV curve.

$$FF = \frac{J_m V_m}{J_{SC} V_{OC}} \tag{9}$$

where J_m and V_m are the highest voltage and current densities at maximum power (P_m) , respectively, which can be extracted from the diagram of I-V.

The most essential metric for a solar cell is its power conversion efficiency (η) . It is the ratio of the cell's maximum output power to the solar power incident on it. It is represented in terms of fill factor by the following formula.

$$\eta = \frac{J_{sc} \times V_{oc} \times FF \times 100\%}{1000[Wm^{-2}] \times Cell\ Area[m^2]}$$

$$\tag{10}$$

The study begins by examining the performance of the initial solar cell configuration with the specified doping concentrations and thicknesses displayed in Fig. 1, as well as the physical parameters of the materials outlined in Table 1. This preliminary analysis is critical for understanding the baseline characteristics of the InGaP solar cell, allowing to establish a comprehensive vision of the doping and thickness ranges that will be explored and optimised in subsequent steps. The following stage involves systematically varying the doping concentration and thickness of each layer in the solar cell: the window layer, the emitter layer, the base layer, and the back surface field (BSF) layer. Each layer is modified across various values to identify the best doping levels and thicknesses to improve solar cell performance. Following the optimisation of each layer, the solar cell's performance has been evaluated and compared. This comparison involves assessing semiconductor parameters such as the J_{sc} , V_{oc} , P_{max} , FF, η , photogeneration rate, and recombination rate. In addition, the external quantum efficiency (EQE) and internal quantum efficiency (IQE) have been evaluated to acquire a better understanding of how successfully solar cell performance is enhanced. Finally, to ensure the quality and performance of the optimised solar cell, its efficiency is compared to that reported in previous research in the literature.

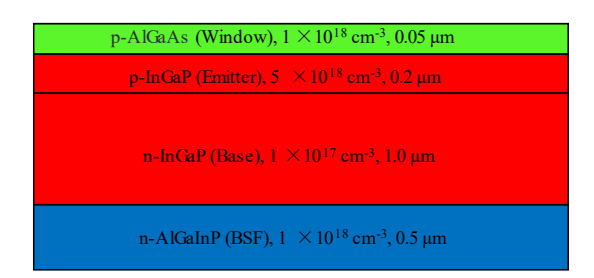


Fig. 1. Initial InGaP solar cell configuration.

Material In_{0.49}Ga_{0.51}P AlGaAs (Al_{0.7}Ga_{0.3})_{0.5}In_{0.5}P Lattice constant (Å) 5.65 2.09 5.65 Energy bandgap (eV) 1.9 11.7 2.4 Permittivity 11.62 3.53 11.7 Affinity (eV) 4.16 212.2 4.2 e- mobility MUN (cm²/Vs) 1945 67.6 2150 1.58e¹⁹ h+ mobility MUP (cm²/Vs) 141 141 $1.3e^{20}$ $1.2e^{20}$ e- density of states NC300 (cm⁻³) $1.5e^{19}$ 1.28e¹⁹ 1e⁻⁹ $1.28e^{19}$ h+ density of states NV300 (cm⁻³) 1e-9 2e-8 1e-9 Lifetime (electrons) TAUN (s) 1e-9 1e⁻⁹ Lifetime (holes) TAUP (s) 2.09

Table 1. Material parameters used in the solar cell simulation [19].

3. Results and Discussion

3.1. Initial solar cell

Figure 2 shows the J-V plot of the initial solar cell as it is retrieved using the Silvaco ATLAS Simulator. From the I-V characteristics, it is found that the J_{sc} is 17.44 mA/cm^2 , V_{oc} is 1.27 V, P_{max} is 18.4 mW/cm^2 , FF is 82.95%, and η is 18.43%.

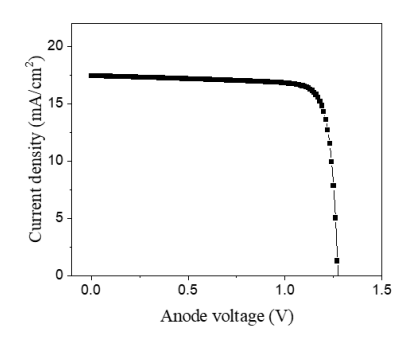
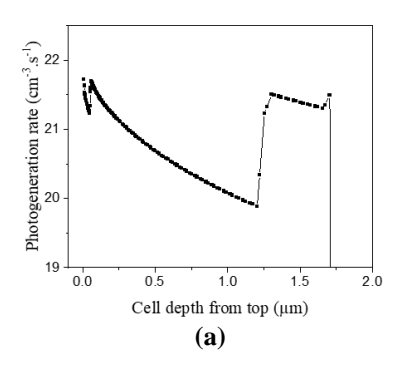


Fig. 2. J-V plot of the initial InGaP solar cell.

Figures 3(a) and (b) depict the photogeneration and recombination rates of the InGaP solar cell, respectively, to gain a deeper comprehension of its initial behaviour. The data presented in Fig. 3(a) indicates that the rate of photogeneration of charged carriers is highest in the upper region of the window, followed by an exponential fall as one moves down the emitter and base regions. Notably, the value of photogeneration increases to a new maximum at the base-BSF boundary. Subsequently, it exhibits a linear decline as it traverses the BSF layer, ultimately reaching its minimum value at the rear surface of the cell. The observed abrupt increase in the photogeneration rate at the boundary layer of the BSF indicates that AlGaInP possesses a notable ability to confine the photogenerated carriers within the cells effectively.

According to Fig. 3(b), the initial cell exhibits an extremely low carrier recombination rate through the window, which can be attributed to its ability to mitigate carrier recombination on the cell's surface. Subsequently, there is a slight rise in recombination in the emitter. In the base region, the recombination rate exhibits a linear increase until reaching its maximum value, after which it decreases to its minimum value at the base-BSF boundary. The carrier recombination rate reaches its highest point in the middle of the BSF layer and then decreases to a minimum rate near the outer boundary of the cell. Comparably, the base region exhibits the lowest generation rate of the carriers and the highest recombination rate. Meanwhile, the InGaAlP BSF layer remarkably impacts recovering the electron-hole pairs toward the active region of the solar cell and minimising the carriers' recombination at the rear side of the cell [20].



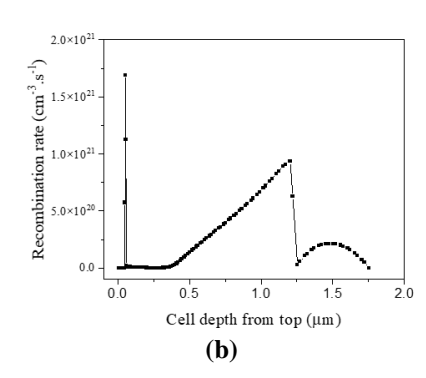


Fig. 3. (a) photogeneration rate and (b) recombination rate versus cell depth of initial InGaP solar cell.

3.2. Optimising the window

The window layer facilitates the absorption of photons with more incredible energy by enabling the transmission of long-wavelength photons to the layer's underneath it. Therefore, it is imperative to regulate the doping concentration and thickness to improve the quantity of photogenerated charges that contribute to the cell's output current, thereby augmenting its efficiency. The window layer's doping concentration is systematically adjusted from 1×10^{18} cm⁻³ to 1×10^{22} cm⁻³, while the thickness is changed from $0.05~\mu m$ to $0.1~\mu m$. The remainder of the regions' parameters remain unaltered from the original cell. Figure 4 illustrates the relationship between conversion efficiency and the window layer's doping level and thickness. Figure 4(a) demonstrates that the efficiency is improved by raising the doping concentration, which is attributed to the enhanced passivation of the front surface of the cell and the reduction of surface recombination. The layer achieves its maximum effectiveness at a doping level of 1×10^{21} cm⁻³. At a higher amount of doping, the layer may exhibit excessive conductivity, leading to the shunt of current away from the active portion of the cell, thus resulting in a decline in efficiency [21].

Figure 4(b) demonstrates a decrease in efficiency with the increase of the window thickness. The efficiency decrement is attributed to a reduction in the intensity of photons that reach the active part of the cell, where the majority of electron-hole pair formation takes place. As a result, less window layer thickness is recommended. According to Fig. 4, the ideal doping level in this work is 1×10^{21} cm $^{-3}$, and the best thickness is $0.05~\mu m$.

The J-V characteristics are plotted using the optimal thickness and doping concentration values of the window layer, as depicted in Fig. 5. In comparison to the initial cell, the J_{sc} rises from 17.44 mA/cm² to 18.46 mA/cm², the V_{oc} is unaffected, the P_{max} rises from 18.4 mW/cm² to 19.57 mW/cm², the FF slightly rises from 82.95% to 83.19%, and the conversion η rises from 18.43% to 19.6%.

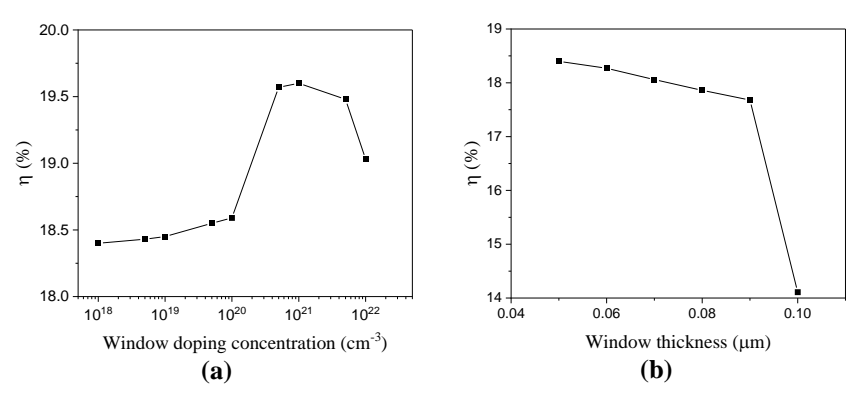


Fig. 4. Efficiency of InGaP solar cell versus window's (a) doping and (b) layer thickness.

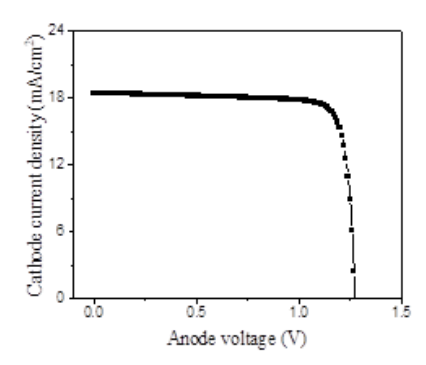


Fig. 5. J-V curve of optimised window layer of the InGaP solar cell.

Figure 6(a) demonstrates that after adjusting the window layer, photogeneration rates in all layers are identical to the starting cell. In contrast, the window layer's recombination rate increases and peaks in its middle, then decreases at the emitter layer boundary (as shown in Fig. 6(b)). The growth of the recombination value in the upper side of the solar cell is correlated to the window doping increases relative to the initial cell during layer optimisation. This causes defects and trap states in the forbidden region that catch electrons and holes and recombine them non-radiatively [22].

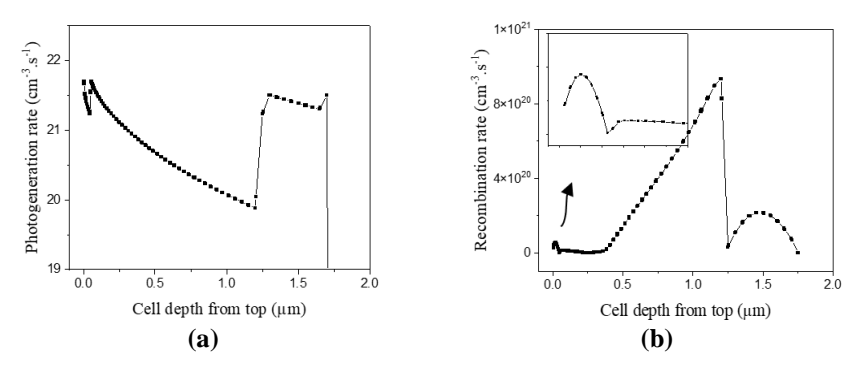


Fig. 6. (a) photogeneration rate and (b) recombination rate along the InGaP solar cell depth after optimising the window layer.

Journal of Engineering Science and Technology December 2024, Vol. 19(6)

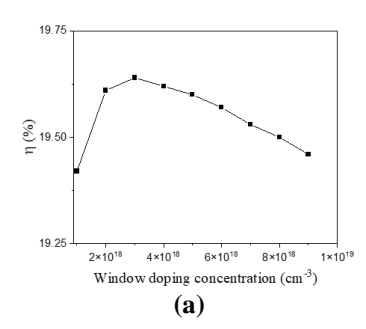
3.3. Optimising the emitter

The study examines the influence of doping level on emitter doping by changing its value from 1×10^{18} cm⁻³ to 9×10^{18} cm⁻³. Figure 7(a) demonstrates that the efficiency exhibits a marginal increase until reaching its peak value of 19.64% at 3×10^{18} cm⁻³ doping concentration and falls for higher concentrations. When emitter doping increases, it creates a doping concentration gradient that raises the electric field within the boundaries of the solar cell layers. This gradient promotes the quick separation of electron-hole pairs, reducing the chance of recombination and increasing solar cell efficiency [23, 24]. Doping at a certain level may cause an increase in recombination rate due to material defects. This may result in a decline in solar cell efficiency.

As light enters a solar cell, electron-hole pairs are produced in the absorber layer. Then, the electron-hole pairs separate, with electrons flowing toward the front electrode and holes heading toward the cell's back contact. The thickness of the emitter layer affects the distance electrons must travel before reaching the external circuit. The impact of emitter thickness is studied by altering between 0.1 and 1 μ m. Figure 7(b) shows that cell efficiency increases until it reaches 21.42% at 0.6 μ m, then decreases as thickness increases. If the emitter layer is too thin, it may be unable to capture all the carriers generated in the absorber layer properly; thus, increasing the emitter thickness improves cell efficiency. When the thickness of the emitter layer surpasses a certain threshold, some electrons may recombine with holes before entering the external circuit. This reduces the efficiency of the solar cell. Figure 7 shows that the optimum doping concentration is 3×10^{18} cm⁻³ and the optimal thickness is 0.6 μ m, respectively.

Figure 8 shows the J-V plot of the InGaP solar cell after optimising the emitter's doping level and thickness. In comparison to the initial cell, the J_{sc} rises from 17.44 mA/cm² to 18.74 mA/cm², the V_{oc} weakly rises from 1.27 V to 1.30 V, the P_{max} rises from 18.4 mW/cm² to 21.39 mW/cm², the FF value increases from 82.95% to 87.57%, and η rises from 18.43% to 21.42%.

Figure 9 shows that after optimising the emitter, the optimised window cell exhibits similar behaviour in terms of photogeneration and recombination rates. Compared to the initial cell, the photogeneration rate has not changed. However, recombination within the emitter occurs faster than in the original cell. This increase is proportional to the width of the emitter after optimisation relative to the starting cell. Increased emitter thickness increases the distance charge carriers must travel to reach the junction, resulting in a shorter carrier lifetime. This increases the possibility of the charge carriers recombining along the way [25].



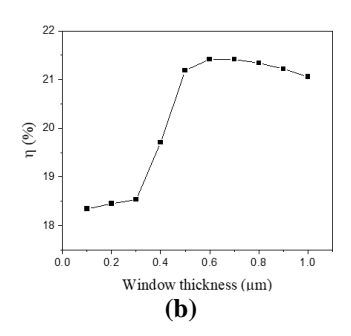


Fig. 7. Efficiency of InGaP solar cell vs. the emitter (a) doping and (b) thickness.

Journal of Engineering Science and Technology December 2024, Vol. 19(6)

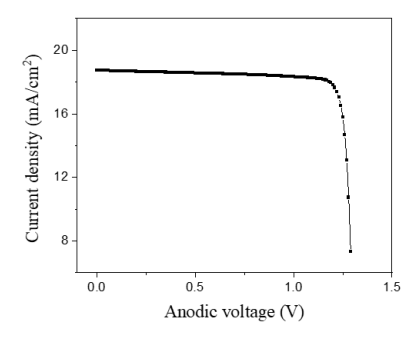
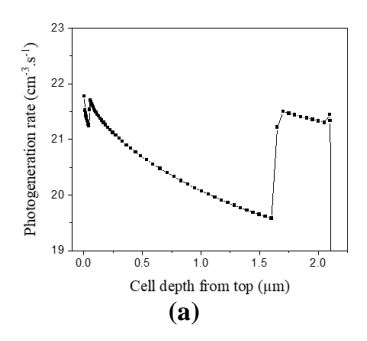


Fig. 8. J-V plot of InGaP solar cell after optimising the emitter layer.



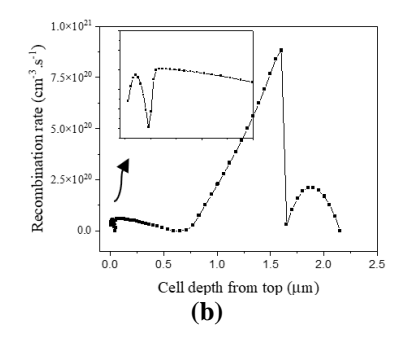
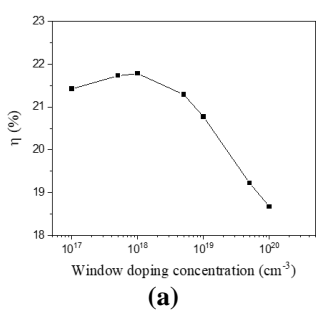


Fig. 9. (a) photogeneration rate and (b) recombination rate as a function of cell depth of InGaP solar cell after optimising the emitter layer.

3.4. Optimising the base

The base layer is critical to the operation of the solar cell because it creates the electric field required to separate the electron-hole pairs produced by incident sunlight. The magnitude of this electric field is proportional to the doping level of the base. To examine the impact of the base doping level on efficiency, the value is changed from 1×10^{17} cm⁻³ to 1×10^{20} cm⁻³. Figure 10(a) illustrates how cell efficiency varies with base layer doping level. The efficiency increases until it reaches the highest value of 21.78% at 1×10^{18} cm⁻³ doping, then falls as the doping level increases [26]. At lower doping concentrations of the base layer, the electric field would be strong enough to separate electron-hole pairs efficiently. When the concentration exceeds 1×10¹⁸ cm⁻³, the electric field becomes excessively strong, leading to increased electron-hole recombination and decreased solar cell efficiency.

Furthermore, the base absorbs the majority of light and collects the majority of photogenerated carriers. Thus, its thickness has a significant impact on cell efficiency. To study the influence of base thickness on InGaP cell efficiency, a range of 0.3 to 1 µm is employed. The results in Fig. 10(b) show that the efficiency improves with the base thickness till reaching the highest value of 26.02% at a thickness of $0.5~\mu m$, then it falls as the thickness increases. As the base thickness rises, more photogenerated carriers are collected. When the thickness crosses a specific threshold, the probability of carrier recombination increases, consequently lowering the efficiency of the solar cell. After optimising the base region, the ideal thickness and doping values are 1×10^{18} cm⁻³ and 0.5 μ m, respectively.



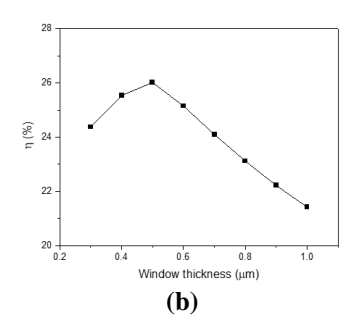


Fig. 10. Efficiency of InGaP solar cell versus the base (a) doping and (b) thickness.

The J-V curve of the InGaP solar cell after optimising the base layer is extracted and plotted, as illustrated in Fig. 11. The J_{sc} rises from 17.44 mA/cm² to 21.19 mA/cm², the V_{oc} rises from 1.27 V to 1.37 V, the P_{max} rises from 18.4 mW/cm² to 26.25 mW/cm², the FF value rises slightly from 82.95% to 90.35%, and η rises from 18.43% to 26.28% in comparison to the initial cell.

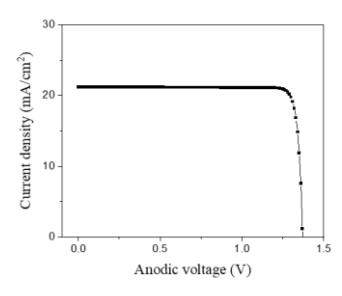
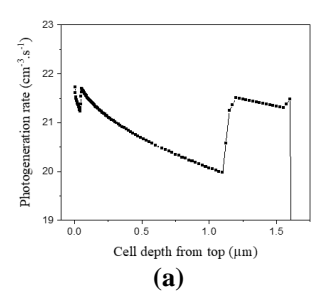


Fig. 11. J-V curve of InGaP solar cell after optimising the base layer.

Again, the cutline of the photogeneration throughout the InGaP solar cell after optimising the base layer is depicted in Fig. 12(a). The recombination rate cutline in Fig. 12(b) shows some decrement in the rate within the base layer as compared to the initial cell. This is due to the base thickness reduction, thus reducing the distance that the carriers need to travel to reach the junction, where they can be separated and supplement the total current of the cell. This minimises the recombination probability of the charge carriers along their path.



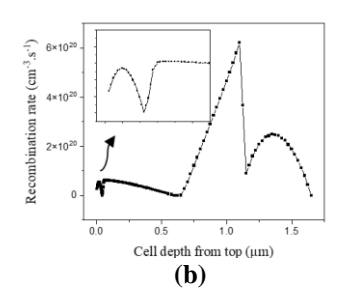


Fig. 12. (a) photogeneration rate and (b) recombination rate versus InGaP solar cell depth after optimising the base layer.

3.5. Optimising the BSF layer

The BSF layer generates an electric field on the cell's rear side, which repels minority carriers and reduces their recombination. The optimisation of BSF doping in the InGaP solar cell is an essential procedure because of its significant influence on the efficiency of the cell. This is achieved by examining the variation in doping levels from 1×10¹⁵ cm⁻³ to 1×10¹⁹ cm⁻³. According to Fig. 13(a), increasing the doping concentration improves cell efficiency. This increase is due to the growing electric field, which decreases the recombination rate and enhances efficiency.

Optimising the BSF layer thickness is crucial for maximising the efficiency of the InGaP solar cell. Figure 13(b) shows the effect of the thickness variation, varied from 0.1 to 1 µm, on the solar cell efficiency. A thicker BSF layer results in muchimproved cell efficiency. As the BSF layer thickness rises, the rate of carrier recombination at the cell's rear surface lowers. This is because the BSF layer contains a more significant concentration of dopants towards the back surface, reducing minority carrier density and improving charge carrier collection [27]. As a result, it enhances the cell performance.

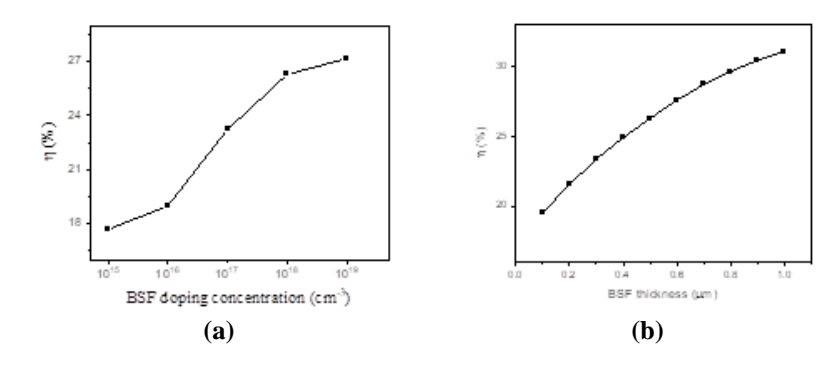


Fig. 13. Efficiency of InGaP solar cell versus BSF (a) doping and (b) thickness.

After Optimising the base layer, the J-V plot of the InGaP solar cell is extracted, as shown in Fig. 14. The J_{sc} increases from 17.44 mA/cm² to 25.8 mA/cm², the V_{oc} rises from 1.27 V to 1.38 V, the P_{max} enhances from 18.4 mW/cm² to 32.05 mW/cm², the FF value enhances from 82.95% to 90.24%, and n improves from 18.43% to 32.09% in comparison to the original cell.

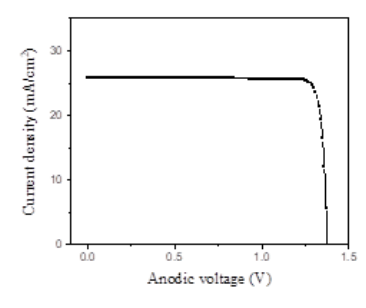


Fig. 14. J-V curve of InGaP solar cell after optimising the BSF layer.

Journal of Engineering Science and Technology December 2024, Vol. 19(6) Again, no change in the photogeneration rate is seen throughout the cell structure after optimising the BSF layer, as shown by the photogeneration rate cutline in Fig. 15(a). However, the recombination rate cutline of the cell after optimising the BSF layer reveals an increase in recombination relative to the original cell, as seen in Fig. 15(b). The high recombination rate is associated with the rise in the doping level and thickness of the BSF layer after optimisation compared to the starting cell. The increase in the BSF doping leads to a surge in the non-radiative recombination, as discussed earlier, and the rise of BSF thickness leads to increases in the distance of the carriers to travel to be collected at the back contact, increases the probability of carriers' recombination rate.

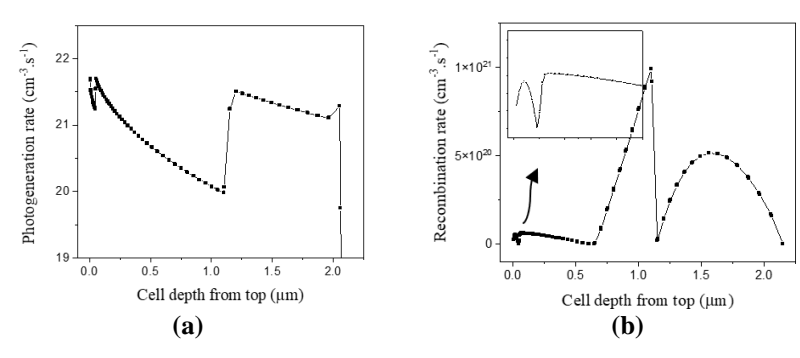


Fig. 15. (a) photogeneration rate and (b) recombination rate versus the InGaP solar cell depth after optimising the BSF layer.

EQE and IQE simulations have been performed to provide detailed information on the usable wavelength range of the InGaP solar cell. EQE is the percentage between the number of carriers a solar cell gathers and the number of photons impinging on it [28]. IQE is the ratio of electron-hole pairs generated to photons absorbed inside the cell's active layer [29]. Figure 16 displays the change in EQE and IQE of the InGaP cell under AM1.5G illumination after optimising each area.

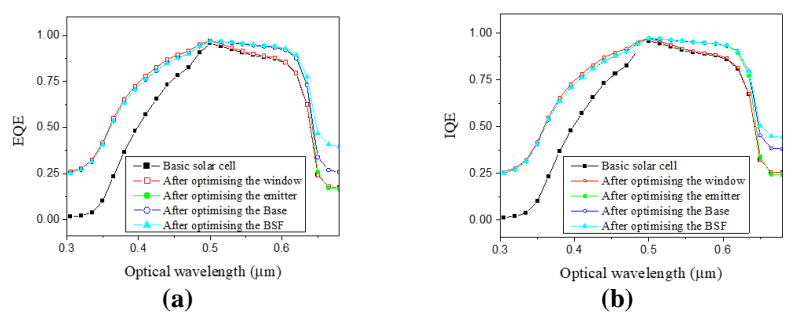


Figure 16. (a) EQE and (b) IQE as a function of irradiation wavelength of InGaP solar cells at different optimising steps.

The InGaP solar cell mainly absorbs photons with wavelengths ranging from 0.3 μm to 0.65 μm , which corresponds to its energy bandgap. The initial cell exhibits a negligible EQE at a wavelength of 0.3 μm . However, following the optimisation of the cell's layers, the EQE at the same wavelength is approximately

26%, suggesting an enhancement in the cell's efficiency. The initial cell and the cell after optimising the window achieve a maximum EQE value of approximately 95.6% at a wavelength of 0.5 µm. However, this value declines linearly to 85% at a wavelength of 0.6 µm. When the emitter, base, and BSF layers are optimised, the solar cells exhibit a peak EQE of 96.8% at a wavelength of 0.5 µm. However, this decreases to 93% at a wavelength of 0.6 µm. This suggests that by optimising the doping and thickness of the emitter, base, and BSF layers, the response of the InGaP solar cell to incident light within the energy bandgap is significantly enhanced. At wavelengths beyond 0.65 µm, the EQE of all cells decreases to a relatively low magnitude. The IQE has a rate of change similar to that of the EQE. However, wavelengths beyond 0.65 µm demonstrate higher values that may be attributed to enhanced carrier movement in the BSF layer [12].

Table 2 presents the enhancements in the characteristics of the InGaP solar cell after optimising each region in the present study. The efficiency of the homojunction In_{0.49}Ga_{0.51}P solar cell in the present study is compared to the reported values in the existing literature, as shown in Table 3. The high efficiency of our optimised solar cell is attributed to the proposed structure, large-scale variation of the thickness and doping concentration of the layers, and the use of the high-energy bandgap AlGaInP as the BSF layer that enhances the confinement of photogenerated carriers within the cell and minimise the recombination rate of the minority carriers, which in turn increases the photogenerated carriers that contribute to the output photocurrent.

Table 2. Electrical parameters of InGaP solar cell after optimising each layer.

Parameter	Initial solar cell	After optimising the window	After optimising the Emitter	After optimising the Base	After optimising the BSF
J_{sc} (mA/cm ²)	17.44	18.46	18.74	21.19	25.8
$V_{oc}(V)$	1.27	1.27	1.30	1.37	1.38
$P_{max} \\ (mW/cm^2)$	18.4	19.57	21.39	26.25	32.05
FF (%)	82.95	83.19	87.57	90.35	90.24
η (%)	18.43	19.6	21.42	26.28	32.09

Table 3. Comparison between the optimised single junction InGaP solar cell and other cells from the literature.

Researcher	Efficiency	Type of Study	
Takamoto et al. [8]	17%	Experimental	
Chang et al. [9]	15.91%	Experimental	
Dai et al. [10]	16.6%	Experimental	
Benlekhdim et al. [11]	18.55%	Simulation	
Verma et al. [12]	21.59%	Simulation	
Soley and Dwivedi [13]	13.42%	Simulation	
Charane et al. [14]	23.73%	Simulation	
Sodabanlu et al. [30]	15.26%	Experimental	
Sodabanlu et al. [31]	15.84%	Experimental	
Sayed and Bedair [32]	14.7%	Simulation	
Djaafar and Hadri [33]	21.87%	Simulation	
Current work	32.09%	Simulation	

4. Conclusions

A single-junction InGaP solar cell configured with AlGaAs (window layer), p-type InGaP (emitter layer), n-type InGaP (base layer), and AlGaInP (BSF layer) has been modelled using Silvaco TCAD. The effect of altering the doping level and thickness of the cell's layers on the electrical characteristics, photogeneration rate, and recombination rate has been thoroughly investigated. The results show that the efficiency gradually increases from 18.43% to 32.09% as the layers are subsequently optimised. The high efficiency of the optimised homojunction In_{0.49}Ga_{0.51}P solar cell in the current study is due to an innovative structural design, careful control over layer thickness and doping concentrations, and strategic use of AlGaInP as the BSF layer. These characteristics improve carrier confinement, reduce recombination losses, and maximise output photocurrent, resulting in improved performance compared to existing solar cells described in the literature. This study emphasises the necessity for more research into the possibility of large band gap InGaP as an appealing active material for solar cells in the coming years.

Acknowledgements

This work was funded by the University of Jeddah, Jeddah, Saudi Arabia, under grant No. (UJ-23-DR-119). Therefore, the authors thank the University of Jeddah for its technical and financial support.

Nomenclatures

FF Fill factor, %

 J_{sc} Short circuit current, mA/cm² P_{Max} Maximum power, mW/cm² V_{oc} Open circuit voltage, V η Conversion efficiency, %

Abbreviations

BSF Back Surface Layer

EQE External Quantum Efficiency IQE Internal Quantum Efficiency

TCAD Technology Computer-Aided Design

References

- 1. Benaicha, M.; Dehimi, L.; Pezzimenti, F.; and Bouzid, F. (2020). Simulation analysis of a high efficiency GaInP/Si multijunction solar cell. *Journal Semiconductors*, 41(3), 032701.
- 2. Kawabata, R.M.S. et al. (2022). III-V SOLAR CELLS. *Journal of Integrated Circuits and Systems*, 17(2), 1-10.
- 3. Bagheri, S.; Talebzadeh, R., Sardari, B.; and Mehdizadeh, F. (2019). Design and simulation of a high efficiency InGaP/GaAs multi junction solar cell with AlGaAs tunnel junction. *Optik*, 199, 163315.
- 4. Mohamed, E.T.; Maka, A.O.M.; Mehmood, M.; Direedar, A.M.; and Amin, N. (2021). Performance simulation of single and dual-junction GaInP/GaAs

- tandem solar cells using AMPS-1D. Sustainable Energy Technologies and Assessments, 44, 101067.
- 5. Li, J.; Wang, J.; Shi, Ch.; Wang, Z.; and Xue, Y.Y. (2020). Research on the emitter thickness optimization of GaInP/GaAs/Ge triple-junction solar cell under space proton based on TCAD simulation. AIP Advances, 10(11), 115110.
- 6. Asmar, J.A. et al. (2015). Power generation and cogeneration management algorithm with renewable energy integration. *Energy Procedia*, 74, 1394-1401.
- Dey, M. et al. (2019). Modelling and simulation of highly efficient single junction gainp solar cell. Proceedings of the 5th International Conference on Advances in Electrical Engineering (ICAEE, 2019), Dhaka, Bangladesh, 609-612.
- Takamoto, T.: Ikeda, E.: Kurita, H.: and Ohmori, M. (1994). Structural optimization for single junction InGaP solar cells. Solar Energy Materials and Solar Cells, 35, 25-31.
- 9. Chang, Y.-A. et al. (2009). Efficiency improvement of single-junction InGaP solar cells fabricated by a novel micro-hole array surface texture process. Semiconductor Science and Technology, 24(8), 085007.
- 10. Dai, P. et al. (2013). The investigation of GaInP solar cell grown by all-solid MBE. Journal of Crystal Growth, 378, 604-606.
- 11. Benlekhdim, A.; Cheknane, A.; Sfaxi, L.; and Hilal, H.S. (2018). Efficiency improvement of single-junction InGaP solar cells by advanced photovoltaic device modelling. Optik, 163, 8-15.
- 12. Verma, M.; Routray, S.R.; and Mishra, G.P. (2021). Analysis and optimization of BSF layer for highly efficient GaInP single junction solar cell. Materials Today: Proceedings, 43(6), 3420-3423.
- 13. Soley, S.S. and Dwivedi, A.D.D. (2021). Numerical simulation and performance analysis of InGaP, GaAs, Ge single junction and InGaP/GaAs/Ge triple junction solar cells. *Materials Today: Proceedings*, 39(5), 2050-2055.
- 14. Charane, H.; Mahrane, A.; Mesrane, A.; and Mazouz, H. (2024) Study and simulation of GaInP single junction solar cell. Engineering Research Express, 6(1), 015076.
- 15. Bakour, A. et al. (2022). Effect and optimization of ZnO layer on the performance of GaInP/GaAs tandem solar cell. Micro and Nanostructures, 168, 207294.
- 16. Mustafa, F.; and Benmoussa, D. (2019). Impact of tunnel heterojunction (InGaP/GaAs) doping concentration on the performance of InGaP/GaAs tandem solar cell using Silvaco-Atlas software. Journal of Ovonic Research, 15(5), 279-285.
- 17. Hossain, J. (2021). Design and simulation of double-heterojunction solar cells based on Si and GaAs wafers. Journal of Physics Communications, 5(8), 085008.
- 18. Wangkheirakpam, V.D.; Bhowmick B.; and Pukhrambam, P.D. (2020). Modelling and simulation of optically Gated TFET for near Infra-Red sensing applications and its low frequency noise analysis. IEEE Sensors Journal, 20(17), 9787-9795.
- 19. Saif, A.A. (2023). High efficiency homojunction GaAs solar cell using InGaP as FSF and AlGaInP as BSF. Results in Optics, 12, 100454.

- 20. Kumari, R.; Mamta; Kumar, R.; and Singh, V.N. (2022). SnTe as a BSF enhances the performance of Sb2Se3 based solar cell: A numerical approach. *Heliyon*, 8(12), e12043.
- 21. Shah, D.K. et al. (2021). A simulation approach for investigating the performances of cadmium telluride solar cells using doping concentrations, carrier lifetimes, thickness of layers, and band gaps. *Solar Energy*, 216, 259-265.
- 22. Mehmood, H.; and Tauqeer, T. (2017). Modelling and performance analysis of amorphous silicon solar cell using wide band gap nc-Si:H window layer. *IET Circuits Devices Systems*, 11(6), 666-675.
- 23. Movla, H.; Shahalizad, A.; and Asgari, A. (2023). A numerical study on the relationship between the doping and performance in P₃HT: PCBM organic bulk heterojunction solar cells. *Scientific Reports*, 13(1), 2031.
- 24. Srivastav, A. et al. (2016). Gradient doping A case study with Ti-Fe2O3 towards an improved photoelectrochemical response. *Physical Chemistry Chemical Physics*, 18(48), 32735-32743.
- 25. Naim, H. et al. (2022). An in-depth optimization of thickness of base and emitter of ZnO/Si heterojunction-based crystalline silicon solar cell: A simulation method. *Journal of Electronic Materials*, 51, 586-593.
- 26. Saif, A.A.; Albishri, M.; Mindil, A.; and Qaeed, M. (2023). Superior efficiency for homojunction GaAs solar cell. *Journal of Ovonic Research*, 19(1), 1-14.
- 27. Karade, V.C. et al. (2022). Combating open circuit voltage loss in Sb₂Se₃ solar cell with an application of SnS as a back surface field layer. *Solar Energy*, 233, 435-445.
- 28. Maka, A.O.M.; and O'Donovan, T.S. (2022). Effect of thermal load on performance parameters of solar concentrating photovoltaic: High-efficiency solar cells. *Energy and Built Environment*, 3(2), 201-209.
- 29. Mohamed, H.A.; Taya, Y.A.; Ali, S.S.; and Mohamed, W.S. (2023). Optical and electrical modeling of CZTSSe based thin-film solar cells. *Physica Scripta*, 98(8), 085516.
- 30. Sodabanlu, H. et al. (2020). High-speed MOVPE growth of InGaP solar cells. *IEEE Journal of Photovoltaics*, 10(2), 480-486.
- 31. Sodabanlu, H.; Li, G.; Watanabe, K.; Nakano, Y.; and Sugiyama, M. (2023). Improvement of InGaP solar cells grown with TBP in planetary MOVPE reactor. *Solar Energy Materials and Solar Cells*, 257, 112402.
- 32. Sayed, I.; and Bedair, S.M. (2019). Quantum well solar cells: Principles, recent progress, and potential. *IEEE Journal of Photovoltaics*, 9(2), 402-423.
- 33. Djaafar, F.; and Hadri, B. (2023). A highly efficient InGaP thin film solar cell structure, optimization and characteristics. *Journal of Renewable Energy and Technology*, 1, 17-23.